# Influence of Substituents on Cation−$\pi$ Interactions. 1. Absolute Binding Energies of Alkali Metal Cation−Toluene Complexes Determined by Threshold Collision-Induced Dissociation and Theoretical Studies

**R. Amunugama and M. T. Rodgers***

*Department of Chemistry, Wayne State University, Detroit, Michigan 48202*

*Received: November 26, 2001; In Final Form: March 19, 2002*

Threshold collision-induced dissociation of $M^+(C_6H_5CH_3)_x$ with Xe is studied using guided ion beam mass spectrometry. $M^+$ include the following alkali metal ions: $Li^+$, $Na^+$, $K^+$, $Rb^+$, and $Cs^+$. Both mono- and bis-complexes are examined (i.e., $x = 1$ and 2). In all cases, the primary and lowest energy dissociation channel observed is endothermic loss of an intact toluene ligand. Sequential dissociation of a second toluene ligand is observed at elevated energies in the bis-complexes. Minor production of ligand exchange products, $M^+Xe$ and $M^+(C_6H_5CH_3)Xe$, is also observed. The cross section thresholds for the primary dissociation channel are interpreted to yield 0 and 298 K bond dissociation energies for $(C_6H_5CH_3)_{x-1}M^+-C_6H_5CH_3$, $x = 1-2$, after accounting for the effects of multiple ion−neutral collisions, the kinetic and internal energies of the reactants, and dissociation lifetimes. Density functional theory calculations at the B3LYP/6-31G* level of theory are used to determine the structures of these complexes and provide molecular constants necessary for the thermodynamic analysis of the experimental data. Theoretical binding energies are determined from single point calculations at the MP2(full)/6-311+G(2d,2p) and B3LYP/6-311+G(2d,2p) levels using the B3LYP/6-31G* geometries. Zero-point energy and basis set superposition error corrections are also included. The agreement between theory and experiment is reasonably good when full electron correlation is included (for $Li^+$, $Na^+$, and $K^+$) but is less satisfactory when effective core potentials are used (for $Rb^+$ and $Cs^+$). In all cases, the experimentally determined bond dissociation energies are greater than the theoretically determined values. In most cases, better agreement is found for the MP2 values than the B3LYP values. The trends in $M^+(C_6H_5CH_3)_x$ binding energies are explained in terms of varying magnitudes of electrostatic interactions and ligand−ligand repulsion in the complexes. Comparisons are also made to previous experimental bond dissociation energies of $M^+(C_6H_6)_x$ to examine the influence of the methyl substituent on the binding, and the factors that control the strength of cation−$\pi$ interactions.

## Introduction

The interaction of metal ions with $\pi$ surfaces of aromatic molecules has become an active area of research interest. Recent reviews of cation−$\pi$ interactions by Dougherty and co-workers provide a detailed overview of cation−$\pi$ interactions, highlighting both the fundamental nature of such interactions and their biological importance.[1,2] Experimental evidence for cation−$\pi$ interactions dates back to much earlier work by Kebarle and co-workers. They found that the interaction of $K^+$ with benzene, a nonpolar molecule, was stronger than the interaction of $K^+$ with water.[18] The interaction is fundamentally of electrostatic nature, between a positively charged metal ion and the electrons that make up the delocalized $\pi$ electron cloud of the aromatic rings. This metal cation−$\pi$ interaction is recognized as a strong noncovalent binding force that plays a dominant role in a wide variety of fields ranging from materials design[3] to molecular biology. Cation−$\pi$ interactions are believed to play an important role in protein structural organization[1,2,4−8] and the functioning of ionic channels in membranes.[9,10] In the nonpolar interior of a protein, these interactions may be significant. Statistically, the aromatic amino acids phenylalanine, tyrosine, and tryptophan comprise 3.9%, 3.2%, and 1.3% of all known proteins, respectively. Therefore, on average, 8.4% of the amino acids residues in any given protein may participate in cation−$\pi$ interactions.[11] This implies that one in every 12 amino acid residues could theoretically engage in such interactions. Of the alkali metal ions, $Na^+$ and $K^+$ are the most biologically relevant.[12] Metal cation−$\pi$ interacting systems involving these ions and some closed-shell nonmetallic cations such as alkylammonium ions have been comprehensively reviewed.[1,2,13] Systems involving other alkali metal ions have thus far received much less attention. For instance, rhodanese, glutamine synthetase, and methylamine dehydrogenase are three protein crystal structures in which the coordination of a $Cs^+$ cation by aromatic residues has been documented. In the structures of glutamine synthetase and methylamine dehydrogenase, the $Cs^+$ cation was used as a heavy-atom replacement by the crystallographers to locate the putative binding site of an $NH_4^+$ cation, whereas the role of the $Cs^+$ cation in rhodanese is not known.[13] Thus, the importance of understanding cation−$\pi$ interactions involving alkali metal ions both from a fundamental perspective as well as the detailed role that they play in biological systems is obvious.

To gain a better understanding of the interaction of alkali metal ions with large biological molecules, knowledge of the structure and energetics of binding to smaller model systems is required. Furthermore, characterizing these interactions in the gas phase is an important and essential part of building a database of information concerning the nature and strength of cation−$\pi$ interactions and the influence of the local environment on such interactions. A number of model systems,[14−22] as well as the aromatic amino acids[23,24] in which the neutral ligand binds

10.1021/jp014307b CCC: $22.00 
Published on Web 05/07/2002

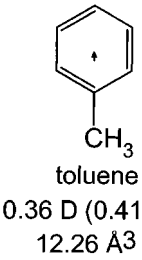


**Figure 1.** Structure of the toluene molecule. The properly scaled dipole moment in Debyes is shown as an arrow. Values listed are taken from experiment[42] and theoretical calculations performed here (in parentheses). The estimated polarizability is also shown.[43]

through its $\pi$ electrons, have been studied in the gas phase. Among the model systems, benzene[14−19] and pyrrole,[20,21] and their derivatives such as phenol and indole,[22] are of particular interest because they constitute the simplest groups of larger aromatic ligands that could mimic the binding properties of complex $\pi$ ligands that might participate in cation−$\pi$ interactions operative in biological systems. Complementary to the gas-phase experimental studies are high-level theoretical calculations, which have been performed for several of the above systems,[1,20−22,25] including alkali metal ion complexes with toluene,[26] at various levels of theory. However, to the best of our knowledge experimental studies on alkali metal cation−$\pi$ interactions with toluene have not been reported in the literature.

In recent work, we have developed methods to allow the application of quantitative threshold collision-induced dissociation (CID) methods to obtain accurate thermodynamic information on increasingly large systems.[17,21,27−41] One of the driving forces behind these developments is our interest in applying such techniques to systems having biological relevance. In addition, we seek to perform accurate thermochemical measurements that provide absolute anchors for metal cation affinity scales over an ever-broadening range of energies and molecular systems. In the present paper, we examine cation−$\pi$ interactions of toluene, $C_6H_5CH_3$, with the alkali metal ions, $Li^+$, $Na^+$, $K^+$, $Rb^+$, and $Cs^+$. The structure of toluene along with its measured[42] and calculated dipole moments (determined here) and estimated polarizability[43] are shown in Figure 1. The kinetic energy-dependent cross sections for CID processes are analyzed using methods developed previously.[31] The analysis explicitly includes the effects of the internal and translational energy distributions of the reactants, multiple ion−neutral collisions, and the lifetime for dissociation. We derive $(C_6H_5CH_3)_{x-1}M^+-C_6H_5CH_3$, $x = 1-2$, bond dissociation energies (BDEs) for all of the complexes and compare these results to ab initio and density functional calculations performed here and in the literature.[26] Comparisons are also made to the analogous benzene systems studied previously[19] to examine the influence of the methyl substituent on the binding, and the factors that control the strength of cation−$\pi$ interactions.

## Experimental Section

**General Procedures.** Cross sections for collision-induced dissociation of $M^+(C_6H_5CH_3)_x$ complexes, where $x = 1-2$, and $M^+ = Li^+$, $Na^+$, $K^+$, $Rb^+$, and $Cs^+$ are measured using a guided ion beam mass spectrometer that has been described in detail previously.[36] The $M^+(C_6H_5CH_3)_x$ complexes are generated in a flow tube ion source by condensation of the alkali metal ion and neutral toluene molecule(s). These complexes are collisionally stabilized and thermalized by $\sim 10^5$ collisions with the He and Ar bath gases such that the internal energies of the ions emanating from the source region are well described by a Maxwell−Boltzmann distribution at room temperature.[36] The ions are extracted from the source, accelerated, and focused into a magnetic sector momentum analyzer for mass analysis. Mass-selected ions are decelerated to a desired kinetic energy and focused into an octopole ion guide, which traps the ions in the radial direction.[44] The octopole passes through a static gas cell containing Xe, used as the collision gas, for reasons described elsewhere.[45−47] Low gas pressures in the cell (typically 0.05−0.20 mTorr) are used to ensure that multiple ion−neutral collisions are improbable. Product and unreacted beam ions drift to the end of the octopole where they are focused into a quadrupole mass filter for mass analysis and subsequently detected with a secondary electron scintillation detector and standard pulse counting techniques.

Ion intensities are converted to absolute cross sections as described previously.[48] Absolute uncertainties in cross section magnitudes are estimated to be ±20%, which are largely the result of errors in the pressure measurement and the length of the interaction region. Relative uncertainties are approximately ±5%. Because the radio frequency used for the octopole does not trap light masses with high efficiency, absolute magnitudes of the cross sections for production of $Li^+$ are probably accurate to ±50%.

Ion kinetic energies in the laboratory frame, $E_{lab}$, are converted to energies in the center of mass frame, $E_{CM}$, using the formula $E_{CM} = E_{lab}m/(m + M)$, where $M$ and $m$ are the masses of the ionic and neutral reactants, respectively. All energies reported below are in the CM frame unless otherwise noted. The absolute zero and distribution of the ion kinetic energies are determined using the octopole ion guide as a retarding potential analyzer as previously described.[48] The distribution of ion kinetic energies is Gaussian with a fwhm between 0.2 and 0.4 eV (lab) for these experiments. The uncertainty in the absolute energy scale is ±0.05 eV (lab).

Because multiple collisions can influence the shape of CID cross sections and the threshold regions are most sensitive to these effects, we have performed pressure-dependent studies of all cross sections examined here. In the present systems, we observe small cross sections at low energies that have an obvious dependence upon pressure. We attribute this to multiple energizing collisions that lead to an enhanced probability of dissociation below threshold as a result of the longer residence time of these slower moving ions. Data free from pressure effects are obtained by extrapolating to zero reactant pressure, as described previously.[49] Thus, results reported below are due to single bimolecular encounters.

**Thermochemical Analysis.** The threshold regions of the reaction cross sections are modeled using eq 1, where $\sigma_0$ is an energy independent scaling factor, $E$ is the relative translational

$$\sigma(E) = \sigma_0 \sum_i g_i (E + E_i - E_0)^n / E \qquad (1)$$

energy of the reactants, $E_0$ is the threshold for reaction of the ground electronic and ro-vibrational state, and $n$ is an adjustable parameter. The summation is over the ro-vibrational states of the reactant ions, $i$, where $E_i$ is the excitation energy of each ro-vibrational state and $g_i$, is the population of those states ($\Sigma g_i = 1$). The populations of excited ro-vibrational levels are not negligible even at 298 K as a result of the many low-frequency modes present in these ions. The relative reactivity of all ro-vibrational states, as reflected by $\sigma_0$ and $n$, is assumed to be equivalent.

The Beyer−Swinehart algorithm[50] is used to evaluate the density of the ro-vibrational states, and the relative populations,

$g_i$ are calculated by an appropriate Maxwell−Boltzmann distribution at the 298 K temperature appropriate for the reactants. The vibrational frequencies of the reactant complexes are determined from density functional theory calculations as discussed in the Theoretical Calculations section. The average vibrational energy at 298 K of the $M^+(C_6H_5CH_3)_x$ complexes is given in the Supporting Information in Table S1. We have estimated the sensitivity of our analysis to the deviations from the true frequencies by scaling the calculated frequencies to encompass the range of average scaling factors needed to bring calculated frequencies into agreement with experimentally determined frequencies found by Pople et al.[51] Thus, the originally calculated vibrational frequencies were increased and decreased by 10%. For the $M^+(C_6H_5CH_3)_x$ complexes with $M^+ = Rb^+$, and $Cs^+$, 20% variations were applied. The corresponding change in the average vibrational energy is taken to be an estimate of one standard deviation of the uncertainty in vibrational energy (Table S1).

We also consider the possibility that collisionally activated complex ions do not dissociate on the time scale of our experiment ($\sim 10^{-4}$ s) by including statistical theories for unimolecular dissociation, specifically Rice−Ramsperger−Kassel−Marcus (RRKM) theory, into eq 1 as described in detail elsewhere.[31,52] The ro-vibrational frequencies appropriate for the energized molecules and the transition states (TSs) leading to dissociation are given in the Supporting Information in Tables S1 and S2. In our analysis, we assume that the TSs are loose and product-like because the interaction between the alkali metal ion and the toluene ligand(s) is largely electrostatic (ion−dipole, ion−induced dipole, and ion−quadrupole interactions). Thus, the most appropriate model for the TS is a loose phase space limit (PSL) model located at the centrifugal barrier for the interaction of $M^+(C_6H_5CH_3)_{x-1}$ with $C_6H_5CH_3$ as described in detail elsewhere.[31] The TS vibrations appropriate for this model are the frequencies of the products, which are also found in Table S1. The transitional frequencies, those that become rotations of the completely dissociated products, are treated as rotors. Two of the transitional mode rotors have rotational constants equal to those of the neutral $C_6H_5CH_3$ product with axes perpendicular to the reaction coordinate, and correspond to its 2-D rotational constant (10.07 $cm^{-1}$). In the $M^+(C_6H_5CH_3)$ systems, which yield one atomic product, these are the only two translational modes. For $M^+(C_6H_5CH_3)_2$ complexes, three additional transitional modes exist. Two of these rotors are the rotational constants of the $M^+(C_6H_5CH_3)$ product, again those with axes perpendicular to the reaction coordinate. Of the two rotational constants of the products with axes lying along the reaction coordinate, one is a transitional mode and is assigned as the remaining rotational constant of the $C_6H_5CH_3$ product (0.185 $cm^{-1}$). The other becomes the 1-D external rotor of the TS. These are listed in Table S2. The 2-D external rotational constants of the TS are determined by assuming that the TS occurs at the centrifugal barrier for interaction of $M^+(C_6H_5CH_3)$ with the neutral $C_6H_5CH_3$ molecule, treated variationally as outlined elsewhere.[31] The 2-D external rotations are treated adiabatically but with centrifugal effects included, consistent with the discussion of Waage and Rabinovitch.[53] In the present work, the adiabatic 2-D rotational energy is treated using a statistical distribution with explicit summation over the possible values of the rotational quantum number, as described in detail elsewhere.[31]

The model represented by eq 1 is expected to be appropriate for translationally driven reactions[54] and has been found to reproduce reaction cross sections well in a number of previous studies of CID processess.[45,49,55−58] The model is convoluted with the kinetic energy distributions of both the reactant ion and neutral Xe atom, and a nonlinear least-squares analysis of the data is performed to give optimized values for the parameters $\sigma_0$, $E_0$, and $n$. The error associated with the measurement of $E_0$ is estimated from the range of threshold values determined for different zero-pressure extrapolated data sets, variations associated with uncertainties in the vibrational frequencies, and the error in the absolute energy scale, 0.05 eV (lab). For analyses that include the RRKM lifetime effect, the uncertainties in the reported $E_0$ values also include the effects of increasing and decreasing the time assumed available for dissociation ($\sim 10^{-4}$ s) by a factor of 2.

Equation 1 explicitly includes the internal energy of the ion, $E_i$. All energy available is treated statistically, which should be a reasonable assumption because the internal (rotational and vibrational) energy of the reactants is redistributed throughout the ion upon impact with the collision gas. The threshold for dissociation is by definition the minimum energy required leading to dissociation, and thus corresponds to formation of products with no internal excitation. The threshold energies for dissociation reactions determined by analysis with eq 1 are converted to 0 K bond energies by assuming that $E_0$ represents the energy difference between reactants and products at 0 K.[59] This assumption requires that there are no activation barriers in excess of the endothermicity of dissociation. This is generally true for ion−molecule reactions[60] and should be valid for the simple heterolytic bond fission reactions examined here.[61]

**Theoretical Calculations.** To obtain model structures, vibrational frequencies, rotational constants, and energetics for the neutral $C_6H_5CH_3$ ligand and for the $M^+(C_6H_5CH_3)_x$ complexes, ab initio and density functional theory calculations were performed using *Gaussian 98*.[62] Geometry optimizations were performed at B3LYP/6-31G* level[63,64] for the $M^+(C_6H_5CH_3)_x$ complexes where $M^+ = Li^+$, $Na^+$, and $K^+$. For complexes containing $Rb^+$ and $Cs^+$, geometry optimizations were performed using a hybrid basis set in which the effective core potentials (ECP) and valence basis sets of Hay and Wadt were used to describe the metal ion,[65] while 6-31G* basis sets were used for C and H atoms. As suggested by Glendening et al.,[66] a single polarization (d) function was added to the Hay−Wadt valence basis set for Rb and Cs, with exponents of 0.24 and 0.19, respectively.

Vibrational analyses of the geometry-optimized structures were performed to determine the vibrational frequencies for the neutral $C_6H_5CH_3$ ligand and the $M^+(C_6H_5CH_3)_x$ complexes for $M^+ = Li^+$, $Na^+$, and $K^+$. The vibrational frequencies for the $M^+(C_6H_5CH_3)_x$ complexes where $M^+ = Rb^+$ and $Cs^+$ were estimated by scaling the calculated frequencies for the analogous $K^+(C_6H_5CH_3)_x$ complexes using a procedure described in detail previously.[67] When used to model data or calculate thermal energy corrections, the calculated vibrational frequencies were scaled by a factor of 0.9804.[68] The vibrational frequencies and rotational constants of neutral $C_6H_5CH_3$ and all $M^+(C_6H_5CH_3)_x$ complexes are listed in the Supporting Information in Tables S1 and S2, respectively. Single point energy calculations were performed at the MP2(full)/6-311+G(2d,2p) and B3LYP/6-311+G(2d,2p) levels using the B3LYP/6-31G* and B3LYP/Hybrid (6-31G*, Hay−Wadt) optimized geometries. To obtain accurate BDEs, zero point energy (ZPE) corrections were applied and basis set superposition errors (BSSE) were subtracted from the computed dissociation energies in the full counterpoise correction.[69,70] The ZPE corrections are small and

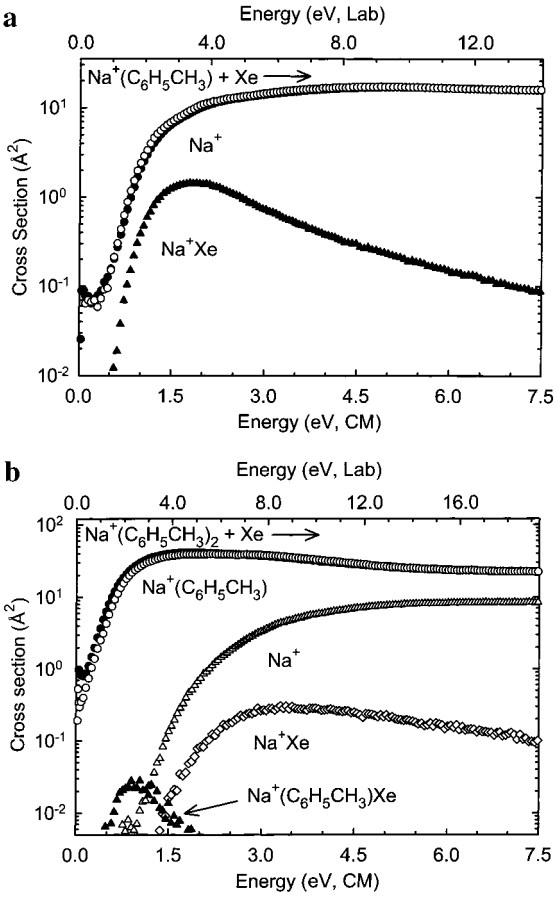


**Figure 2.** Cross sections for collision-induced dissociation of $Na^+(C_6H_5CH_3)_x$, $x = 1$ and 2 (parts a and b, respectively), with Xe as a function of kinetic energy in the center-of-mass frame (lower *x*-axis) and the laboratory frame (upper *x*-axis). Data are shown for a Xe pressure of ~0.2 and ~0.1 mTorr, for the $x = 1$ and 2 complexes, respectively. Primary and secondary product cross sections are shown as ● and △, respectively. Primary and secondary ligand exchange product cross sections are shown as ▲ and ◇, respectively. Data are also shown for the primary product cross section, extrapolated to zero pressure of Xe as ○.

decrease with increasing size of the alkali metal ion, and are 7.5, 4.1, 3.1, 2.5, and 2.3 kJ/mol for the $M^+(C_6H_5CH_3)$ complexes and 3.4, 2.8, 2.6, 2.8, and 2.8 kJ/mol for the $M^+(C_6H_5CH_3)_2$ complexes, where $M^+ = Li^+$, $Na^+$, $K^+$, $Rb^+$, and $Cs^+$, respectively. The BSSE corrections are small and range from 0.6 to 3.1 kJ/mol for the B3LYP values but are significantly larger and range from 5.8 to 21.2 kJ/mol for the MP2 values.

## Results

**Cross Sections for Collision-Induced Dissociation.** Experimental cross sections were obtained for the interaction of Xe with ten $M^+(C_6H_5CH_3)_x$ complexes, where $M^+ = Li^+$, $Na^+$, $K^+$, $Rb^+$, and $Cs^+$, and $x = 1$ and 2. Figure 2 shows representative data for the $Na^+(C_6H_5CH_3)_x$, $x = 1$ and 2 complexes. The other $M^+(C_6H_5CH_3)_x$ complexes show relative behavior similar to that of $Na^+(C_6H_5CH_3)_x$, and are included in the Supporting Information as Figure S1. The sequential loss of intact toluene molecules and ligand exchange with Xe are the only processes observed in these systems over the collision energy range studied, typically 0 to >5 eV. The primary (most favorable) process observed for all of these complexes is the loss of a single intact toluene molecule in the CID reactions 2.

$$M^+(C_6H_5CH_3)_x + Xe \rightarrow M^+(C_6H_5CH_3)_{x-1} + C_6H_5CH_3 + Xe \quad (2)$$

The maximum cross section for reaction 2, as well as the total cross section, roughly doubles in magnitude from the mono- to the bis-complexes. The threshold for reaction 2 also decreases from the mono- to bis-complexes, consistent with conventional ideas of ligation of gas-phase ions, i.e., stepwise sequential bond energies decrease because of increasing electrostatic repulsion between the ligands, causing the distance between the cation and ligands to increase. Such ideas have been noted in previous experimental and theoretical studies of $M^+(ligand)_n$ clusters.[40,41,71−74]

**$M^+(C_6H_5CH_3)$ + Xe.** Results for the interaction of $Na^+(C_6H_5CH_3)$ with Xe are shown in Figure 2a. The major product is $Na^+$. The $Na^+$ product cross section has an apparent threshold of 0.3 eV and exhibits a maximum cross section of ~14 Å$^2$. The apparent thresholds for the analogous CID process in the other $M^+(C_6H_5CH_3)$ complexes decrease regularly as the size of the cation increases, such that $Li^+(C_6H_5CH_3)$ exhibits the largest apparent threshold of 1.8 eV, and $Cs^+(C_6H_5CH_3)$ the smallest apparent threshold of 0.1 eV. In general, the cross sections maxima for other $M^+(C_6H_5CH_3)$ increase with the size of the cation, such that cross section maxima is the smallest for $Li^+(C_6H_5CH_3)$, ~3 Å$^2$, and the largest for $Cs^+(C_6H_5CH_3)$, ~27 Å$^2$. The $Rb^+(C_6H_5CH_3)$ complex deviates from this simple trend, exhibiting a maximum cross section intermediate between that observed for the $Li^+$ and $Na^+$ complexes. The ligand exchange product $Na^+Xe$ is observed with an apparent threshold of 0.6 eV and a maximum cross section of 1.4 Å$^2$ at 1.8 eV, which drops off rapidly with energy due to competition with the primary CID process. The apparent thresholds for the analogous ligand exchange process in the other $M^+(C_6H_5CH_3)$ complexes decrease regularly as the size of the cation increases, such that $Li^+Xe$ exhibits the largest apparent threshold of 1.5 eV, and $Cs^+(C_6H_5CH_3)$ the smallest apparent threshold of 0.2 eV. The cross section maxima for other $M^+Xe$ products are all small and range from 0.3 to 0.9 Å$^2$ for other $M^+(C_6H_5CH_3)$ complexes. It is possible that competition between the primary CID process and the ligand exchange reaction could shift the apparent threshold for the primary CID process to higher energies than the true thermodynamic threshold, a competitive shift. However, as the cross sections for ligand exchange processes are at least an order of magnitude smaller than those for the primary CID processes, we do not believe this competition has an appreciable effect on the thresholds measured here for the primary dissociation processes of these complexes.

The apparent thresholds for the $M^+Xe$ ligand exchange product from the CID of all $M^+(C_6H_5CH_3)$ complexes, are near or above those of the primary dissociation products, $M^+$ (Figure 2a and S1). The true thermodynamic thresholds of these channels are lower than those of the primary dissociation channel by the $M^+-Xe$ binding energy.[75] However, this is not always evident in the apparent thresholds, because of the large difference in the relative magnitudes of the cross sections for these channels.

**$M^+(C_6H_5CH_3)_2$ + Xe.** Results of the interaction of $Na^+(C_6H_5CH_3)_2$ with Xe are shown in Figure 2b. The primary product observed at all energies is $Na^+(C_6H_5CH_3)$, corresponding to loss of an intact $C_6H_5CH_3$ molecule. The $Na^+(C_6H_5CH_3)$ product has an apparent threshold near or below 0 eV, such that the cross section is nonzero at 0 eV. The apparent threshold for the analogous CID process in the other $M^+(C_6H_5CH_3)_2$ complexes exhibit similar behavior in that the cross section magnitude is

**TABLE 1: Fitting Parameters of Eq 1, Threshold Dissociation Energies at 0 K, and Entropies of Activation at 1000 K[a]**

| reactant complex | $\sigma_0$[b] | $n$[b] | $E_0$[c] (eV) | $E_0$(PSL) (eV) | kinetic shift (eV) | $\Delta S^\dagger$(PSL) (J mol$^{-1}$ K$^{-1}$) |
|---|---|---|---|---|---|---|
| $Li^+(C_6H_5CH_3)$ | 1.1(0.1) | 1.7(0.1) | 2.09(0.16) | 1.90(0.17) | 0.19 | 55(2) |
| $Na^+(C_6H_5CH_3)$ | 15.6(0.2) | 1.2(0.1) | 1.18(0.04) | 1.16(0.03) | 0.02 | 50(2) |
| $K^+(C_6H_5CH_3)$ | 21.8(0.4) | 1.1(0.1) | 0.84(0.04) | 0.83(0.03) | 0.01 | 44(2) |
| $Rb^+(C_6H_5CH_3)$ | 10.8(0.6) | 1.1(0.1) | 0.74(0.03) | 0.74(0.04) | 0.00 | 53(2) |
| $Cs^+(C_6H_5CH_3)$ | 21.0(1.7) | 1.3(0.1) | 0.66(0.03) | 0.66(0.03) | 0.00 | 57(2) |
| $Li^+(C_6H_5CH_3)_2$ | 58.3(1.5) | 1.0(0.1) | 1.36(0.04) | 1.21(0.02) | 0.15 | 59(4) |
| $Na^+(C_6H_5CH_3)_2$ | 63.5(1.4) | 1.1(0.1) | 0.97(0.04) | 0.90(0.02) | 0.07 | 40(5) |
| $K^+(C_6H_5CH_3)_2$ | 74.4(3.9) | 0.9(0.1) | 0.82(0.04) | 0.78(0.05) | 0.04 | 25(5) |
| $Rb^+(C_6H_5CH_3)_2$ | 43.9(0.7) | 0.9(0.1) | 0.72(0.04) | 0.70(0.02) | 0.02 | 27(5) |
| $Cs^+(C_6H_5CH_3)_2$ | 58.2(1.7) | 1.0(0.2) | 0.66(0.03) | 0.64(0.03) | 0.02 | 29(5) |

[a] Uncertainties are listed in parentheses. [b] Average values for loose PSL transition state. [c] No RRKM analysis.

nonzero at 0 eV for all of the alkali metal ions except $Li^+$, which exhibits an apparent threshold of ~0.3 eV. In fact, the cross section magnitude at 0 eV and all energies is found to increase with increasing size of the metal ion and is more than twice as large as that measured for the monoligated systems. However, the $Rb^+$ system again deviates from this trend, exhibiting a cross section that is smaller than for any of the other metal ions. The maximum cross section observed varies from 32 to 46 Å$^2$ across these systems. The cross section for the primary product is observed to decline as the secondary CID product, $Na^+$, is formed indicating that this product is formed sequentially from the primary CID product. The $Na^+$ product has an apparent threshold of 0.9 Å$^2$ and reaches a maximum cross section of ~7 Å$^2$ at the highest energies examined. The other $M^+(C_6H_5CH_3)_2$ complexes show similar relative behavior such that the primary product declines as the secondary CID product, $M^+$, appears. The cross sections maxima of the secondary CID products vary from 2 to 14 Å$^2$ across these systems.

In addition to the CID processes, ligand exchange reactions are also observed, producing both the primary ligand exchange product, $Na^+(C_6H_5CH_3)Xe$, as well as the secondary ligand exchange product $Na^+Xe$ (Figure 2b). The primary ligand exchange product, $Na^+(C_6H_5CH_3)Xe$ has an apparent threshold near 0.5 eV, reaches a maximum cross section of ~0.03 Å$^2$, and then falls off rapidly due to competition with the primary CID process as well as sequential dissociation to produce the secondary ligand exchange product, $Na^+Xe$. The secondary ligand exchange product, $Na^+Xe$, slowly grows in from an apparent threshold of ~1.4 Å$^2$, and reaches a maximum cross section of ~0.3 Å$^2$ at approximately 3.3 eV. At higher energies, it falls off due to competition with the secondary CID process. The other $M^+(C_6H_5CH_3)_2$ complexes show similar relative ligand exchange behavior; however, the reactant ion beam intensities were much smaller for the $Rb^+(C_6H_5CH_3)_2$ and $Cs^+(C_6H_5CH_3)_2$ complexes making it impossible to distinguish the primary ligand exchange product, $M^+(C_6H_5CH_3)Xe$, from noise in these systems. The cross sections magnitudes of the ligand exchange products are quite small. The primary and secondary ligand exchange products are approximately 3 and 2 orders of magnitude smaller than the primary CID product, respectively.

**Threshold Analysis.** The model of eq 1 was used to analyze the thresholds for reactions 2 in ten $M^+(C_6H_5CH_3)_x$ systems. As previously discussed,[52,76] the analysis of the primary CID thresholds provides the most reliable thermochemistry for such CID studies. This is because secondary and higher order products are more sensitive to lifetime effects, and additional assumptions are needed to quantitatively include the multiple products formed. The results of these analyses are given in Table 1 for all ten $M^+(C_6H_5CH_3)_x$ complexes. Representative fits using eq 1 for $Na^+(C_6H_5CH_3)_x$, $x = 1$ and 2, are shown in Figure 3. A comparable set of figures for the other eight $M^+(C_6H_5CH_3)_x$ complexes are available in the Supporting Information as Figure S2. Experimental cross sections for the primary dissociation processes of the $M^+(C_6H_5CH_3)_x$ complexes are accurately reproduced using a loose PSL TS model.[31] This model has been shown to provide the most accurate determination of kinetic shifts for CID reactions for electrostatically bound metal−ligand complexes.[27,31,57,58,77−80] The data are accurately reproduced over energy ranges exceeding 1 eV and over cross section magnitudes of a factor of at least 100 for all complexes except $Rb^+(C_6H_5CH_3)_2$ and $Cs^+(C_6H_5CH_3)_2$. Threshold values, $E_0$, obtained from analyses of the data without consideration of lifetime effects are also included in Table 1. The difference between these values

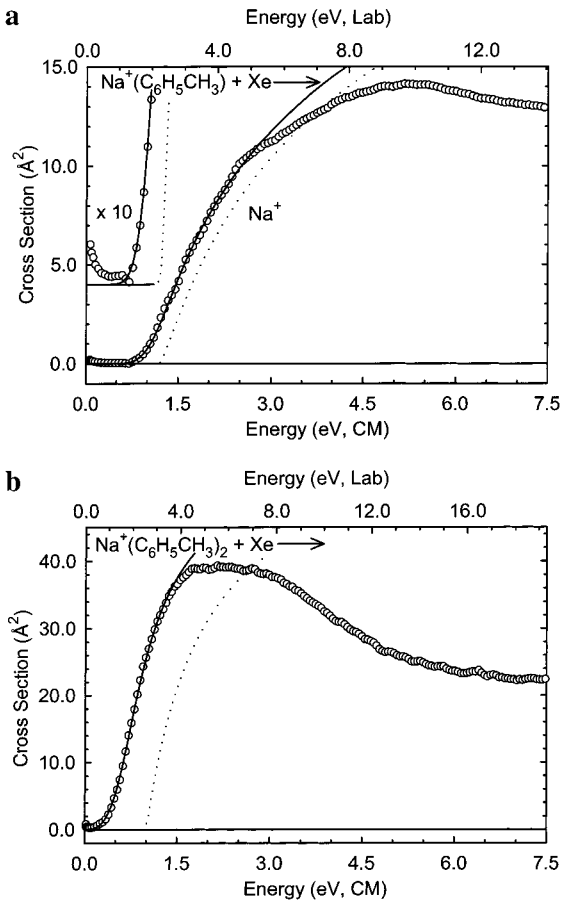


**Figure 3.** Zero-pressure extrapolated cross sections for the primary collision-induced dissociation product of the $Na^+(C_6H_5CH_3)_x$ complexes, $x = 1$ and 2 (parts a and b, respectively), with Xe in the threshold region as a function of kinetic energy in the center-of mass frame (lower $x$-axis) and the laboratory frame (upper $x$-axis). Solid lines show the best fits to the data using the model of eq 1 convoluted over the neutral and ion kinetic and internal energy distributions. Dashed lines show the model cross sections in the absence of experimental kinetic energy broadening for reactants with an internal energy of 0 K.

**TABLE 2: Geometrical Parameters of B3LYP/6-31G* Optimized Structures of the $M^+(C_6H_5CH_3)_x$ Complexes**

| complex | M−C (Å) | M−centroid (Å)[a] | C−C (Å) | C−H (Å) | C−H OOP angle (deg)[b] | C−$CH_3$ (Å) | C−H (Å)[d] |
|---|---|---|---|---|---|---|---|
| $C_6H_5CH_3$ | | | 1.398 | 1.080 | 0.04 | 1.510 | 1.090 |
| $Li^+(C_6H_5CH_3)$ | 2.335 | 1.867 | 1.408 | 1.080 | 0.32 | 1.510 | 1.090 |
| $Na^+(C_6H_5CH_3)$ | 2.747 | 2.366 | 1.406 | 1.080 | 0.30 | 1.510 | 1.090 |
| $K^+(C_6H_5CH_3)$ | 3.186 | 2.865 | 1.403 | 1.080 | 0.24 | 1.510 | 1.090 |
| $Rb^+(C_6H_5CH_3)$[c] | 3.466 | 3.167 | 1.403 | 1.080 | 0.20 | 1.510 | 1.090 |
| $Cs^+(C_6H_5CH_3)$[c] | 3.736 | 3.456 | 1.402 | 1.080 | 0.15 | 1.510 | 1.090 |
| $Li^+(C_6H_5CH_3)_2$ | 2.481 | 2.051 | 1.404 | 1.080 | 0.26 | 1.510 | 1.090 |
| $Na^+(C_6H_5CH_3)_2$ | 2.816 | 2.444 | 1.404 | 1.080 | 0.21 | 1.510 | 1.090 |
| $K^+(C_6H_5CH_3)_2$ | 3.233 | 2.917 | 1.403 | 1.080 | 0.23 | 1.510 | 1.090 |
| $Rb^+(C_6H_5CH_3)_2$[c] | 3.498 | 3.208 | 1.402 | 1.080 | 0.17 | 1.510 | 1.090 |
| $Cs^+(C_6H_5CH_3)_2$[c] | 3.759 | 3.490 | 1.402 | 1.080 | 0.15 | 1.510 | 1.090 |

[a] The metal−ring-centroid distance is defined as the distance from the metal atom to the central point within the aromatic ring of toluene that is in the plane of the carbon atoms. [b] Out-of-plane angle. [c] The Hay−Wadt ECP/valence basis set was used for the metal ion, as described in the text, and the 6-31G* basis set for C and H. [d] Bond length of C−H in methyl group.

and those obtained when lifetime effects are included, $E_0$(PSL), the kinetic shift, is also given in Table 1. The kinetic shifts observed for these systems vary from 0.0 to 0.19 eV for the $M^+(C_6H_5CH_3)$ complexes with 42 vibrational modes, and from 0.02 to 0.15 eV for the $M^+(C_6H_5CH_3)_2$ complexes that have 87 vibrational modes. The kinetic shifts decrease with increasing size of the cation, from $Li^+$ to $Cs^+$, in both the mono- and bis-ligated complexes. This is easily understood because the observed kinetic shift should directly correlate with the density of states of the complex at threshold, which depends on the measured BDE, as shown in Table 1.

We also examined the influence of treating the vibrations associated with the methyl torsions as free rotors. This treatment produced a very small effect on the threshold values determined as a result of cancellation of competing effects. Treating the methyl torsions as free rotors increases the amount of energy available to the complex, increases the number of states available at the transition state, and increases the density of states of reactant complex. The first two effects tend to lead to an increase in the threshold, while the third leads to a decrease in the threshold. Overall, these effects nearly cancel and produce a negligible effect on the threshold determined.

The entropy of activation, $\Delta S^\dagger$, is a measure of the looseness of the transition state. It is also a reflection of the complexity of the system because it is largely determined by the molecular parameters used to model the energized molecule and the TS but also depends on the threshold energy. The $\Delta S^\dagger$(PSL) values at 1000 K are listed in Table 1 and vary between 25 and 59 J $K^{-1}$ $mol^{-1}$. These entropies of activation compare favorably to an expanding range of noncovalently bound metal−ligand complexes previously measured in our laboratory and to those collected by Lifshitz for simple bond cleavage reactions of ions.[81]

**Theoretical Results.** Theoretical structures for neutral toluene and for the mono- and bis-ligated complexes of toluene with $Li^+$, $Na^+$, $K^+$, $Rb^+$, and $Cs^+$ were calculated as described above. Details of the geometry-optimized structures for each of these species are given in Table 2. The most stable structures for $Na^+(C_6H_5CH_3)$ and $Na^+(C_6H_5CH_3)_2$ are shown in Figure 4. The metal atom binds to the $\pi$ cloud of the aromatic ring of toluene molecule, a cation−$\pi$ interaction. The distortion of the toluene molecule that occurs upon complexation to the alkali metal ion is minor. The change in geometry is largest for $Li^+$ and decreases with increasing size of the metal ion. The C−C bond lengths in the aromatic ring of toluene were found to increase by 0.004−0.010 Å upon complexation to the alkali metal ion as compared to the free ligand, Table 2. The alkali metal ion appears to have no influence on the aromatic ring C−H bond length (1.080 Å), methyl C−H bond length (1.090 Å), and

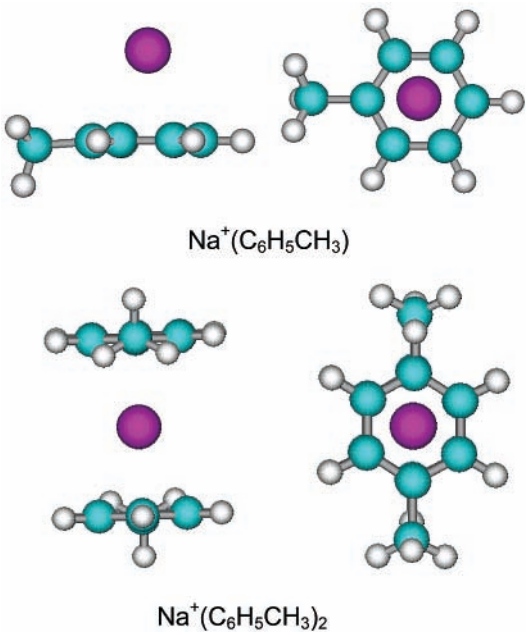


**Figure 4.** B3LYP/6-31G* optimized geometries of $Na^+(C_6H_5CH_3)_x$ complexes, where $x = 1-2$. Two views of each optimized structure are shown.

C−$CH_3$ bond length (1.510 Å). As summarized in Table 2, the $M^+$−C and $M^+$−ring-centroid distances[82] are found to increase as the size of the metal ion increases from $Li^+$ to $Cs^+$ for both the mono- and bis-ligated complexes. The $M^+$−C and $M^+$−ring-centroid distances are also found to increase on going from the mono-ligated to the corresponding bis-ligated complex for all metal ions as expected for electrostatically bound complexes. In contrast to that found for the analogous benzene systems,[19] out of plane bending of the ring hydrogen atoms is found to decrease with increasing size of the alkali metal ion, and is larger for the mono-ligated complexes that for the bis-ligated complexes. This makes sense because the alkali metal ion is further away from the ring and, therefore, these hydrogen atoms in the complexes to the larger metal ions. The metal ion is also further from these atoms in the bis-ligated complexes than in the mono-ligated complexes, and should therefore exert a smaller influence.

As can be seen in Figure 4, the lowest energy structure for the $Na^+(C_6H_5CH_3)_2$ complex has the methyl substituents oriented anti to one another to minimize repulsive ligand−ligand interactions associated with the methyl substituents. The anti configuration was found to be the lowest energy structure for all of the bis-ligated complexes. To estimate the barrier to free rotation of the aromatic ring in the bis-ligated complex,

**TABLE 3: Bond Dissociation Enthalpies of $M^+(C_6H_5CH_3)_x$, $x = 1-2$, at 0 K in kJ/mol**

| | | | theory, X = $CH_3$ | | | | | | | |
|---|---|---|---|---|---|---|---|---|---|---|
| | experiment (TCID) | | MP2 | | | B3LYP | | | literature (MP2) | |
| complex | X = $CH_3$[a] | X = H[b] | $D_e$[c] | $D_0$[c,d] | $D_{0,BSSE}$[c,e] | $D_e$[f] | $D_0$[d,f] | $D_{0,BSSE}$[e,f] | $D_0$[g] | $D_{0,BSSE}$[g] |
| $Li^+(C_6H_5X)$ | 183.1(16.0) | 161.1(13.5) | 173.3 | 165.8 | 155.8 | 173.8 | 166.4 | 164.8 | 160.2 | 159.0 |
| $Na^+(C_6H_5X)$ | 112.3(3.5) | 92.6(5.8)<br>88.3(4.3)[h] | 112.8 | 108.7 | 98.3 | 109.8 | 105.7 | 102.7 | 97.9 | 96.7 |
| $K^+(C_6H_5X)$ | 79.9(5.0) | 73.3(3.8) | 86.5 | 83.4 | 77.6 | 73.9 | 70.8 | 69.8 | | |
| $Rb^+(C_6H_5X)$[i] | 71.3(4.2) | 68.5(3.8) | 71.2 | 68.7 | 61.3 | 54.7 | 52.2 | 51.6 | | |
| $Cs^+(C_6H_5X)$[i] | 64.0(4.4) | 64.6(4.8) | 62.9 | 60.6 | 53.4 | 44.7 | 42.4 | 40.3 | | |
| $Li^+(C_6H_5X)_2$ | 116.5(2.7) | 104.2(6.8) | 137.7 | 134.3 | 113.1 | 95.9 | 92.6 | 90.0 | | |
| $Na^+(C_6H_5X)_2$ | 86.6(2.3) | 80.0(5.8) | 102.4 | 99.6 | 83.9 | 81.3 | 78.5 | 75.4 | | |
| $K^+(C_6H_5X)_2$ | 75.1(4.6) | 67.5(6.8) | 79.1 | 76.5 | 66.3 | 58.3 | 55.6 | 54.0 | | |
| $Rb^+(C_6H_5X)_2$i | 67.7(4.2) | 62.7(7.7) | 71.5 | 68.7 | 57.4 | 45.4 | 42.6 | 41.9 | | |
| $Cs^+(C_6H_5X)_2$i | 61.6(4.0) | 58.8(7.7) | 61.4 | 58.6 | 49.3 | 37.7 | 34.8 | 34.2 | | |

[a] Present results, threshold collision-induced dissociation. Uncertainties are listed in parentheses. [b] Taken from Amicangelo and Armentrout, except as noted.[19] [c] Calculated at the MP2(full)/6-311+G(2d, 2p) level of theory using B3LYP/-31G* optimized geometries. [d] Including zero point energy corrections with B3LYP/6-31G* frequencies scaled by 0.9804. [e] Also includes basis set superposition error corrections. [f] Calculated at B3LYP/6-311+G(2d, 2p) level of theory using B3LYP/6-31G* optimized geometries. [g] Tsuzuki et al. calculated at the MP2/6-311G**//MP2/6-311G** level of theory.[26] [h] Armentrout and Rodgers.[17] [i] The Hay−Wadt ECP/valence basis set was used for the metal ion, as described in the text, and the 6-31G* basis set and 6-311+G(2d, 2p) basis set were used for C and H in geometry optimization and single point energy calculation, respectively.

optimizations were also performed for $Li^+(C_6H_5CH_3)_2$ with the methyl groups oreinted syn, "ortho", and "meta" to one another. These complexes were found to be 0.4, 1.2, and 0.1 kJ/mol less stable than the ground state complex, respectively. Therefore, at room temperature these complexes should have sufficient energy to freely interconvert (see Table S1).

Theoretical estimates for the $M^+(C_6H_5CH_3)_x$ BDEs were determined using the B3LYP/6-31G* geometries and single point energy calculations at both the MP2(full)/6-311+G(2d, 2p) and B3LYP/6-311+G(2d, 2p) levels of theory. These results are listed in Table 3 along with the experimental determinations performed here for toluene, and other theoretical results found in the literature.[24] Results shown in Table 3 also include ZPE and BSSE corrections. The values calculated at these levels of theory differ somewhat and are greater for the bis-ligated complexes than for the mono-ligated complexes. The mean absolute deviation (MAD) for all 10 complexes is 11.9 ± 5.3 kJ/mol, whereas it is somewhat smaller for the mono-ligated complexes, 8.8 ± 3.2 kJ/mol, and larger for the bis-ligated complexes, 14.9 ± 5.4 kJ/mol. In general, the MP2 values are larger than the B3LYP values except for the $Li^+(C_6H_5CH_3)$ and $Na^+(C_6H_5CH_3)$ complexes. Previous calculations for these two complexes performed at the MP2/6-311G** level of theory employing optimized structures calculated at the same level of theory by Tsuzuki et al.[26] differ somewhat from the values obtained here. Their BDE for the $Li^+$ complex lies 3.2 kJ/mol above our MP2 value and 5.8 kJ/mol below our B3LYP value. In contrast, the BDE they determine for the $Na^+$ complex lies below both values computed here, by 1.6 kJ/mol below the MP2 value and 6.0 kJ/mol below the B3LYP value. These differences are quite reasonable, based upon the expected accuracy of these levels of theory.

## Discussion

**Trends in Experimental $M^+(C_6H_5CH_3)_x$ Bond Dissociation Energies.** The experimental BDEs of the $M^+(C_6H_5CH_3)_x$ complexes at 0 K are summarized in Table 3. The variation in the measured BDEs with the size of the alkali metal ion are shown in Figure 5 for both the mono- and bis-complexes. The $M^+-(C_6H_5CH_3)$ and $(C_6H_5CH_3)M^+-(C_6H_5CH_3)$ BDEs are found to decrease monotonically as the size of the alkali metal increases from $Li^+$ to $Cs^+$. This is the expected trend for binding

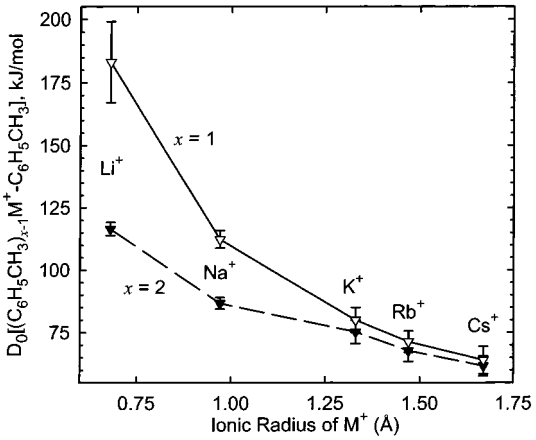


**Figure 5.** Bond dissociation energies at 0 K (in kJ/mol) of the $M^+(C_6H_5CH_3)_x$ complexes plotted versus the ionic radius of $M^+$. Data are shown for $x = 1$ and 2 as ▽ and ▼, respectively. All values are taken from Table 3.

based primarily on electrostatic interactions (ion−dipole, ion−induced dipole and ion−quadrupole),[1] because the increasing size of the alkali metal ion[83] leads to larger metal−ligand bond distances (see Table 2). Also, the difference in BDEs for adjacent metals becomes smaller as the size of the metal ion increases from $Li^+$ to $Cs^+$ for both the $M^+(C_6H_5CH_3)$ and $M^+(C_6H_5CH_3)_2$ complexes. This trend results from a combination of two factors. First, the relative changes in ionic radii for the alkali-metal cations becomes smaller as the size of the alkali metal ion increases (0.68, 0.97, 1.33, 1.47, and 1.67 Å for $Li^+$, $Na^+$, $K^+$, $Rb^+$, and $Cs^+$, respectively).[83] Second, the nonlinear distance dependencies of the electrostatic interactions fall off rapidly as $r^{-2}$ for ion−dipole, as $r^{-3}$ for the ion−quadrupole and as $r^{-4}$ for ion−induced dipole interactions.

The BDEs of the bis-ligated complexes are smaller than the BDEs for the corresponding mono-ligated complexes in all cases. The decrease in the measured BDE on going from the mono- to bis-ligated system is largest for the $Li^+$ complex, and decreases with increasing size of the alkali metal ion. The sequential BDE is observed to decrease by 66.6, 25.7, 4.8, 3.6, and 2.4 kJ/mol for the $Li^+$, $Na^+$, $K^+$, $Rb^+$, and $Cs^+$ systems, respectively. This trend is believed to be the result of Coulombic and dipole−dipole repulsion between the ligands.[77] Using the

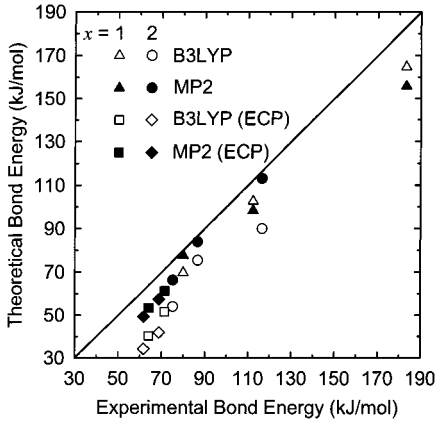


**Figure 6.** Theoretical versus experimental bond dissociation energies at 0 K (in kJ/mol) of the $M^+(C_6H_5CH_3)_x$ complexes. The diagonal line indicates the values for which the calculated and measured bond dissociation energies are equal. All values are taken from Table 3.

$M^+$−centroid distances provided in Table 2, the distances between the aromatic rings are found to increase with increasing size of the alkali metal ion, from ∼4.10 Å in $Li^+(C_6H_5CH_3)_2$ to 7.00 Å in $Cs^+(C_6H_5CH_3)_2$. Thus, the magnitude of the repulsive ligand−ligand interactions should also decrease with increasing size of the alkali metal ion. This should result in a smaller difference in the BDEs for the mono- and bis-complexes with increasing size of the alkali metal ion as observed. The very small differences observed for the $K^+$, $Rb^+$, and $Cs^+$ systems suggest that the ligand−ligand repulsion is very similar and minor for these complexes.

**Comparison of Theory and Experiment.** The experimentally determined and theoretically calculated $M^+(C_6H_5CH_3)_x$ BDEs are listed in Table 3. The agreement between the experimental BDEs and theoretical values determined at the MP2(full)/6-311+G(2d, 2p)//B3LYP/6-31G* and B3LYP/6-311+G(2d,2p)//B3LYP/6-31G* levels is illustrated in Figure 6. In general, the theoretical calculations are in qualitative agreement with all of the observed trends in the experimental BDEs discussed in the previous section. Quantitatively, the agreement between the experimental and the six theoretical $M^+(C_6H_5CH_3)_x$ BDEs calculated including all electrons ($M^+ = Li^+$, $Na^+$, $K^+$, $x = 1$ and 2) is reasonably good, with a mean absolute deviation (MAD) of 9.8 ± 9.7 kJ/mol for the MP2 BDEs and 16.1 ± 6.9 kJ/mol for the B3LYP BDEs. These differences are somewhat larger than the average experimental error in these values of 5.7 ± 5.2 kJ/mol. The low theoretical BDEs for $Li^+(C_6H_5CH_3)$ as compared to the experimental value (a difference of 27.3 and 18.3 kJ/mol for the MP2 and B3LYP values, respectively) is disappointing. If these values are not included, the MAD drops to is 6.2 ± 5.1 kJ/mol for the MP2 values and 15.7 ± 7.7 kJ/mol for the B3LYP values. This poorer agreement may arise for two reasons. The first is the experimental difficulty in measuring cross sections for $Li^+$ as a result of the difficulty associated with efficient detection of this light mass.[84] An alternative explanation is that theory may systematically underestimate the bond energies for $Li^+$ complexes, as a result of the higher degree of covalency in the metal−ligand bond. This is shown by the calculated partial charge on $M^+$, which is 0.77*e* for $Li^+(C_6H_5CH_3)$ and varies between 0.89 and 0.99*e* for all of the other $M^+(C_6H_5CH_3)_x$ complexes at the MP2 level. Therefore, higher levels of theory may be required to accurately describe the binding in this complex, a conclusion also drawn for $Li^+$ complexes with a variety of other ligands.[34,36,38]

The agreement between the experimental BDEs and the theoretical values calculated using the Hay−Wadt ECP/valence basis set for the metal ions ($Rb^+$ and $Cs^+$) is not as good. A MAD of 10.8 ± 1.0 kJ/mol is found for the MP2 values, whereas a MAD of 24.2 ± 3.3 kJ/mol is found for the B3LYP values. It is clear from Table 3 and Figure 6 that the Hay−Wadt ECP/valence basis set results in calculated BDEs that are too low and that the deviations are larger for $Cs^+$ than $Rb^+$. These observations suggest that, the Hay−Wadt ECP/valence basis set introduces systematic errors in the determination of alkali metal binding affinities to toluene. Similar results were found for the analogous benzene systems.[19] Overall, these results suggest that the level of theory employed here is inadequate for determination of accurate alkali metal binding affinities of ligands to $Rb^+$ and $Cs^+$ ions.

**Conversion from 0 to 298 K.** To allow comparison to commonly used experimental conditions, we convert the 0 K bond energies determined here to 298 K bond enthalpies and free energies. The enthalpy and entropy conversions are calculated using standard formulas (assuming harmonic oscillator and rigid rotor models) and the vibrational and rotational constants determined for the B3LYP/6-31G* optimized geometries, which are given in the Supporting Information in Tables S1 and S2. Table 4 lists 0 and 298 K enthalpies, free energies, and enthalpic and entropic corrections for all systems experimentally determined (from Table 1). The uncertainties in the enthalpic and entropic corrections are determined by 10% variation in the molecular constants for complexes to $Li^+$, $Na^+$, and $K^+$, and by 20% variation in the molecular constants for complexes to $Rb^+$ and $Cs^+$. Because the metal−ligand frequencies are very low and may not be adequately described by theory, the listed uncertainties also include contributions from scaling these frequencies up and down by a factor of 2. The latter provides a conservative estimate of the computational errors in these low-frequency modes and is the dominant source of the uncertainties listed.

**TABLE 4: Enthalpies and Free Energies Binding of $M^+(C_6H_5CH_3)_x$, $x = 1-2$, at 0 and 298 K in kJ/mol[a]**

| reactant complex | $\Delta H_0$[b] | $\Delta H_{298} - \Delta H_0$[c] | $\Delta H_{298}$ | $T\Delta S_{298}$[c] | $\Delta G_{298}$ |
|---|---|---|---|---|---|
| $Li^+(C_6H_5CH_3)$ | 183.1(16.0) | 3.3(3.0) | 186.4(16.3) | 36.3(6.4) | 150.1(17.5) |
| $Na^+(C_6H_5CH_3)$ | 112.3(3.5) | 1.5(3.0) | 113.8(4.6) | 33.9(9.1) | 79.9(10.2) |
| $K^+(C_6H_5CH_3)$ | 79.9(5.0) | 0.9(1.7) | 80.8(5.3) | 31.9(7.8) | 48.9(9.4) |
| $Rb^+(C_6H_5CH_3)$ | 71.3(4.2) | 0.9(1.7) | 72.2(4.6) | 33.7(7.8) | 38.5(9.0) |
| $Cs^+(C_6H_5CH_3)$ | 64.0(4.4) | 0.9(1.7) | 64.9(4.7) | 34.5(7.8) | 30.4(9.1) |
| $Li^+(C_6H_5CH_3)_2$ | 116.5(2.7) | −2.8(2.1) | 113.7(3.4) | 43.5(12.9) | 70.2(13.3) |
| $Na^+(C_6H_5CH_3)_2$ | 86.6(2.3) | −3.0(1.7) | 83.6(2.8) | 38.0(13.3) | 45.6(13.6) |
| $K^+(C_6H_5CH_3)_2$ | 75.1(4.6) | −3.0(1.3) | 72.1(4.8) | 33.8(13.4) | 38.3(14.3) |
| $Rb^+(C_6H_5CH_3)_2$ | 67.7(4.2) | −3.6(1.2) | 64.1(4.4) | 30.1(13.5) | 34.0(14.2) |
| $Cs^+(C_6H_5CH_3)_2$ | 61.6(4.0) | −3.0(1.2) | 58.6(4.2) | 34.5(13.4) | 24.1(14.1) |

[a] Uncertainties are listed in parentheses. [b] Present experimental results (Table 3). [c] Density functional values from calculations at the B3LYP/6-31G* level of theory with frequencies scaled by 0.9804. The Hay−Wadt ECP/valence basis set was used for $Rb^+$ and $Cs^+$.

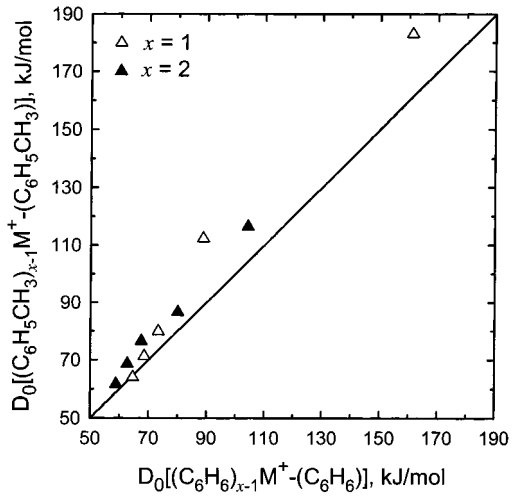


**Figure 7.** Experimental bond dissociation energies (in kJ/mol) at 0 K of the $(C_6H_5CH_3)_{x-1}M^+-(C_6H_5CH_3)$ vs $(C_6H_6)_{x-1}M^+-(C_6H_6)$, where $M^+ = Li^+$, $Na^+$, $K^+$, $Rb^+$, and $K^+$. Data are shown for $x = 1$ and 2 as △ and ▲, respectively. All values are taken from Table 3.

**Influence of the Methyl Substituent.** The effect of the methyl substituent on the cation−$\pi$ interaction can be examined by comparing the results obtained here for toluene, $C_6H_5CH_3$, to those obtained in an earlier study for benzene, $C_6H_6$.[19] Benzene is a highly symmetric molecule and has no dipole moment. Methyl substitution breaks up the symmetry in the molecule, resulting in a modest dipole moment for toluene. The measured value for the dipole moment of toluene is 0.36 ± 0.05 D,[42] in good agreement with the value determined from the theoretical calculations performed here, 0.41 D. However, the dipole moment lies in the plane of the aromatic ring and is therefore an effective interaction of the alkali metal ion with the dipole moment is not possible in cation−$\pi$ complexes to toluene. The polarizability of benzene is estimated using the additivity method of Miller[43] to be 9.99 Å$^3$ and increases to 12.26 Å$^3$ for toluene. Therefore, the ion−induced dipole interaction should be slightly stronger for complexes to toluene than to benzene. Dougherty and co-workers have argued that to first order, the major aspect of the cation−$\pi$ interaction results from interaction of the cation with the large permanent quadrupole moment of the aromatic ligand.[1,2,9] Benzene is found to have a large negative quadrupole moment of (−8.69 DÅ) that results from the delocalized $\pi$ electron density above and below the plane of the aromatic ring.[85] Established techniques for measuring the quadrupole moment require that the molecule has no dipole moment, and therefore, the quadrupole moment of toluene has not been measured. However, methyl substituents are generally referred to as electron donors because their presence leads to an increase in the electron density of the aromatic $\pi$ system. Therefore, methyl substitution should result in a larger quadrupole moment for toluene as compared to benzene. As discussed above, a cation−$\pi$ interaction between an alkali metal ion and an aromatic ligand is expected to be largely electrostatic, arising from ion−dipole, ion−induced dipole, and ion−quadrupole interactions, but dominated by the ion−quadrupole interaction. Thus, all three of the above effects of methyl substitution should act in concert to increase the strength of the cation−$\pi$ interaction in the complexes examined here. Indeed, this is exactly what is observed as shown in Table 3 and Figure 7. The measured BDEs of the $M^+(C_6H_5CH_3)_x$ complexes are observed to be larger than those of the $M^+(C_6H_6)_x$ complexes in all cases except $Cs^+(C_6H_5CH_3)$. In this case, the measured BDE of $Cs^+(C_6H_5CH_3)$ is 64.0 ± 4.4 kJ/mol, whereas the measured BDE of $Cs^+(C_6H_6)$ is 64.6 ± 4.8 kJ/mol. The difference in the measured BDEs, 0.6 kJ/mol, is significantly smaller than the experimental errors in these measurements suggesting that we cannot conclusively establish that the binding in the complex to toluene is weaker. To examine this in more detail, we performed ligand exchange experiments to establish which complex binds more strongly. These experiments are analogous to the CID experiments discussed in the Experimental Section except that, the neutral CID gas, Xe, was replaced by benzene and toluene as shown in reactions 3a and 3b.

$$M^+(C_6H_6) + C_6H_5CH_3 \rightarrow M^+(C_6H_5CH_3) + C_6H_6 \quad (3a)$$

$$M^+(C_6H_5CH_3) + C_6H_6 \rightarrow M^+(C_6H_6) + C_6H_5CH_3 \quad (3b)$$

The measured rate for the ligand exchange cross section is converted to a rate constant as described previously.[48,86] The ratio of the rate constants for reactions 3a and 3b can then be equated to the equilibrium constant for ligand exchange, $K = k_{3a}/k_{3b}$ and thus provides a direct measure of the differences in the free energy of binding to these ligands, $\Delta G_{298K}$. In this way, we measure an equilibrium constant of $K = 3.2 \pm 1.6$, which can be converted to a free energy difference of $\Delta G_{298K} = 2.9 \pm 1.0$ kJ/mol in favor of toluene. This difference is within the experimental error of either measurement, is well within the combined experimental errors of the two CID measurements, and definitively establishes that toluene binds more strongly to $Cs^+$ than benzene. Thus, we can conclude that methyl substitution leads to an enhancement in the cation−$\pi$ interaction in all cases as expected based upon the dipole moments, quadrupole moments, and polarizabilities of benzene and toluene. The enhancement in the binding energy is greatest for the $Li^+$ complexes and decreases with increasing size of the cation. Likewise, the enhancement in binding is greater for the mono-ligated complexes than for the bis-ligated complexes, particularly for the complexes to $Li^+$ and $Na^+$. Because only two aromatic systems are compared here, it is impossible to separate out the influence that each of these effects, the dipole moment, polarizability, and quadrupole moment, has on the cation−$\pi$ interaction. To better understand the relative influence that each of these effects have upon cation−$\pi$ interactions, we are engaging in parallel studies involving of a variety of other aromatic ligands that will be the subject of future manuscripts.

## Conclusions

The kinetic energy dependence of the collision-induced dissociation of $M^+(C_6H_5CH_3)_x$ complexes ($M^+ = Li^+$, $Na^+$, $K^+$, $Rb^+$, and $Cs^+$, $x = 1$ and 2), with Xe is examined in a guided ion beam tandem mass spectrometer. The dominant dissociation pathway observed for all complexes, mono- and bis-ligated, is loss of an intact toluene molecule. Thresholds for these dissociation reactions are determined after careful consideration of the effects of reactant internal energy, multiple collisions with Xe, and the lifetime of the ionic reactants (using a loose phase space limit transition state model). Molecular parameters needed for the analysis of experimental data as well as structures and theoretical estimates of the bond dissociation energies for the $M^+(C_6H_5CH_3)_x$ complexes are obtained from theoretical calculations performed at the MP2(full)/6-311+G(2d,2p)//B3LYP/6-31G* and B3LYP/6-311+G(2d,2p)//B3LYP/6-31G* levels. The absolute $M^+-(C_6H_5CH_3)$ and $(C_6H_5CH_3)M^+-(C_6H_5CH_3)$ bond dissociation energies as well as the change in sequential $M^+(C_6H_5CH_3)_x$ ($x = 1-2$) bond dissociation energies are observed to decrease monotonically as the size of the alkali

metal ion increases from $Li^+$ to $Cs^+$. These trends are explained in terms of the electrostatic nature of the bonding in the $M^+(C_6H_5CH_3)_x$ complexes and the changes in magnitude of the repulsive ligand−ligand interactions in the $M^+(C_6H_5CH_3)_2$ complexes, respectively. Theoretical values of the $M^+(C_6H_5CH_3)_x$ bond energies are also determined by ab initio and density functional calculations performed at the MP2(full)/6-311+G(2d,2p)//B3LYP/6-31G* and B3LYP/6-311+G(2d,2p)//B3LYP/6-31G* levels of theory for $M^+ = Li^+$, $Na^+$, and $K^+$. The agreement between theory and experiment is reasonably good when full electron correlation is included, for $Li^+$, $Na^+$, and $K^+$. However, significant deviations are observed for the monoligated $Li^+$ ion complex. When effective core potentials are used, for $Rb^+$ and $Cs^+$, theory is found to significantly underestimate the strength of the binding. In all cases, the experimentally determined bond dissociation energies are greater than the theoretically determined values. In general, MP2 theory is able to more accurately describe the binding in these systems than B3LYP. The trends in $M^+(C_6H_5CH_3)_x$ binding energies are explained in terms of varying magnitudes of electrostatic interactions and ligand−ligand repulsion in the complexes. Comparisons made to experimental BDEs of the analogous benzene complexes reveal that the methyl substituent leads to an increase in the strength of the cation−$\pi$ interaction, in both the mono- and bis-ligated complexes, to all of the alkali metal ions.

**Acknowledgment.** This work was supported by the National Science Foundation, Grant No. 0138504, and in part by an ASMS Research Award from Micromass.

**Supporting Information Available:** Tables of vibrational frequencies, average vibrational energies and rotational constants, and B3LYP/6-31G* geometry optimized structures for neutral $C_6H_5CH_3$ and the $M^+(C_6H_5CH_3)_x$ complexes. Figures showing cross sections for the collision-induced dissociation of $M^+(C_6H_5CH_3)_x$ complexes with Xe as well as empirical fits to the primary product channels (PDF). This material is available free of charge via the Internet at http://pubs.acs.org.

**Note Added after ASAP Posting.** This article was released ASAP on 5/7/2002 before author corrections were included. The corrected manuscript was posted 5/8/2002.

## References and Notes

(1) Ma, J. C.; Dougherty, D. A. *Chem. Rev.* **1997**, *97*, 1303.
(2) Dougherty, D. A. *Science* **1996**, *271*, 163.
(3) *Metal-Ion Separation and Preconcentration*; Bond, A. H., Dietz, M. L., Rodgers, R. D., Eds.; ACS Symposium Series 716; American Chemical Society: Washington, DC, 1999.
(4) DeVos, A. M.; Ultsch, M.; Kossiakoff, A. A. *Science* **1992**, *255*, 306.
(5) Karlin, A. *Curr. Opin. Neurobiol.* **1993**, *3*, 299.
(6) Raves, M. L.; Harel, M.; Pang, Y. P.; Silman, I.; Kozikowski, A. P.; Sussman, J. L. *Nat. Struct. Biol.* **1997**, *4*, 57.
(7) Stauffer, D. A.; Karlin, A. *Biochemistry* **1994**, *33*, 6840.
(8) Mitchell, J. B.; Nandi, C. L.; McDonald, I. K.; Thornton, J. M.; Price, S. L. *J. Mol. Biol.* **1994**, *239*, 315.
(9) Zhong, W.; Gallivan, J. P.; Zhang, Y.; Li, L.; Lester, H. A.; Dougherty, D. A. *Proc. Natl. Acad. Sci. U.S.A.* **1998**, *95*, 12088.
(10) Donini, O.; Weaver, D. F. *J. Comput. Chem.* **1998**, *19*, 1515.
(11) Meadows, E. S.; De Wall, S. L.; Barbour, L. J.; Gokel, G. W. *J. Am. Chem. Soc.* **2001**, *123*, 3092.
(12) *Principles of Bioinorganic Chemistry*; Lippard, S. J., Berg, J. M., Eds.; University Science Books: Mill Valley, CA, 1994.
(13) Gokel, G. W.; De Wall, S. L.; Meadows, E. S. *Eur. J. Org. Chem.* **2000**, 2967.
(14) Woodin, R. L.; Beauchamp, J. L. *J. Am. Chem. Soc.* **1978**, *100*, 501.
(15) Taft, R. W.; Anvia, F.; Gal, J.-F.; Walsh, S.; Capon, M.; Holmes, M. C.; Hosn, K.; Oloumi, G.; Vasanwala, R.; Yazdani, S. *Pure Appl. Chem.* **1990**, *62*, 17.
(16) Guo, B. C.; Purnell, J. W.; Castleman, Jr., A. W. *Chem. Phys. Lett.* **1990**, *168*, 155.
(17) Armentrout, P. B.; Rodgers, M. T. *J. Phys. Chem. A* **2000**, *104*, 2238.
(18) Sunner, J.; Nishizawa, K.; Kebarle, P. *J. Phys. Chem.* **1981**, *85*, 1814.
(19) Amicangelo, J. C.; Armentrout, P. B. *J. Phys. Chem. A* **2000**, *104*, 11420.
(20) Gapeev, A.; Yang, C.-Y.; Klippenstein, S. J.; Dunbar, R. C. *J. Phys. Chem. A* **2000**, *104*, 3246.
(21) Huang, H.; Rodgers, M. T. *J. Phys. Chem. A* **2002**, *106*, 4277.
(22) Ryzhov, V.; Dunbar, R. C. *J. Am. Chem. Soc.* **1999**, *121*, 2259.
(23) Ryzhov, V.; Dunbar, R. C.; Cerda, B.; Wesdemiotis, C. *J. Am. Soc. Mass Spectrom.* **2000**, *11*, 1037.
(24) Gapeev, A.; Dunbar, R. C. *J. Am. Chem. Soc.* **2001**, *123*, 8360.
(25) Feller, D.; Dixon, D. A.; Nicholas, J. B. *J. Phys. Chem. A* **2000**, *104*, 11414.
(26) Tsuzuki, S.; Yoshida, M.; Uchimaru, T.; Mikami, M. *J. Phys. Chem. A* **2001**, *105*, 769.
(27) Rodgers, M. T.; Armentrout, P. B. *J. Phys. Chem. A* **1997**, *101*, 1238.
(28) Rodgers, M. T.; Armentrout, P. B. *J. Phys. Chem. A* **1997**, *101*, 2614.
(29) Rodgers, M. T.; Armentrout, P. B. *J. Phys. Chem. A* **1999**, *103*, 4955.
(30) Rodgers, M. T.; Armentrout, P. B. *J. Chem. Phys.* **1998**, *109*, 1787.
(31) Rodgers, M. T.; Ervin, K. M.; Armentrout, P. B. *J. Chem. Phys.* **1997**, *106*, 4499.
(32) Rodgers, M. T.; Armentrout, P. B. *Intl. J. Mass Spectrom.* **1999**, *185/186/187*, 359.
(33) Amunugama, R.; Rodgers, M. T. *Int. J. Mass Spectrom.* **2000**, *195/196*, 439.
(34) Rodgers, M. T.; Armentrout, P. B. *J. Am. Chem. Soc.* **2000**, *122*, 8548.
(35) Rodgers, M. T.; Stanley, J. R.; Amunugama, R. *J. Am. Chem. Soc.* **2000**, *122*, 10969.
(36) Rodgers, M. T. *J. Phys. Chem. A* **2001**, *105*, 2374.
(37) Amunugama, R.; Rodgers, M. T. *J. Phys. Chem. A* **2001**, *105*, 9883.
(38) Rodgers, M. T. *J. Phys. Chem. A* **2001**, *105*, 8145.
(39) Rodgers, M. T.; Armentrout, P. B. *J. Am. Chem. Soc.* **2002**, *124*, 2678.
(40) Valina, A. B.; Amunugama, R.; Huang, H.; Rodgers, M. T. *J. Phys. Chem. A* **2001**, *105*, 11057.
(41) Vitale, G.; Valina, A. B.; Huang, H.; Amunugama, R.; Rodgers, M. T. *J. Phys. Chem. A* **2001**, *105*, 11351.
(42) *Handbook of Chemistry and Physics*; Weast, R. C., Astle, M. J., Eds.; CRC Press: Boca Raton, FL, 1982; p E-61.
(43) Miller, K. J. *J. Am. Chem. Soc.* **1990**, *112*, 8533.
(44) Teloy, E.; Gerlich, D. *Chem. Phys.* **1974**, *4*, 417. Gerlich, D., Diplomarbeit, University of Freiburg, Federal Republic of Germany, 1971. Gerlich, D. In *State-Selected and State-to-State Ion−Molecule Reaction Dynamics, Part I, Experiment;* Ng, C.-Y., Baer, M., Eds.; Advances in Chemical Physics Series; Wiley: New York, 1992; Vol. 82, p 1.
(45) Dalleska, N. F.; Honma, K.; Armentrout, P. B. *J. Am. Chem. Soc.* **1993**, *115*, 12125.
(46) Aristov, N.; Armentrout, P. B. *J. Phys. Chem.* **1986**, *90*, 5135.
(47) Hales, D. A.; Armentrout, P. B. *J. Cluster Sci.* **1990**, *1*, 127.
(48) Ervin, K. M.; Armentrout, P. B. *J. Chem. Phys.* **1985**, *83*, 166.
(49) Dalleska, N. F.; Honma, K.; Sunderlin, L. S.; Armentrout, P. B. *J. Am. Chem. Soc.* **1994**, *116*, 3519.
(50) Beyer, T. S.; Swinehart, D. F.; *Comm. Assoc. Compt. Machines* **1973**, *16*, 379. Stein, S. E.; Rabinovitch, B. S. *J. Chem. Phys.* **1973**, *58*, 2438; *Chem. Phys. Lett.* **1977**, *49*, 1883.
(51) Pople, J. A.; Schlegel, H. B.; Ragavachari, K.; deFrees, D. J.; Binkley, J. F.; Frisch, M. J.; Whitesides, R. F.; Hout, R. F.; Hehre, W. J. *Int. J. Quantum Chem. Symp.* **1981**, *15*, 269. DeFrees, D. J.; Mclean, A. D. *J. Chem. Phys.* **1985**, *82*, 333.
(52) Khan, F. A.; Clemmer, D. C.; Schultz, R. H.; Armentrout, P. B. *J. Phys. Chem.* **1993**, *97*, 7978.
(53) Waage, E. V.; Rabinovitch, B. S. *Chem. Rev.* **1970**, *70*, 377.
(54) Chesnavich, W. J.; Bowers, M. T. *J. Phys. Chem.* **1979**, *83*, 900.
(55) Schultz, R. H.; Crellin, K. C.; Armentrout, P. B. *J. Am. Chem. Soc.* **1991**, *113*, 8590.
(56) More, M. B.; Gledening, E. D.; Armentrout, P. B. *J. Phys. Chem.* **1996**, *100*, 1605.
(57) Ray, D.; Feller, D.; More, M. B.; Gledening, E. D.; Armentrout, P. B. *J. Phys. Chem.* **1996**, *100*, 16116.
(58) Meyer, F.; Khan, F. A.; Armentrout, P. B. *J. Am. Chem. Soc.* **1995**, *117*, 9740.
(59) See, for example, Figure 1 in Dalleska et al.[45]

(60) Armentrout, P. B. In *Advances in Gas-Phase Ion Chemistry*; Adams, N. G., Babcock, L. M., Eds.; JAI: Greenwich, 1992; Vol. 1, pp 83−119.
(61) Armentrout, P. B.; Simons, J. *J. Am. Chem. Soc.* **1992**, *114*, 8627.
(62) Frisch, M. J.; Trucks, G. W.; Schlegel, H. B.; Scuseria, G. E.; Robb, M. A.; Cheeseman, J. R.; Zakrzewski, V. G.; Montgomery Jr., J. A.; Stratmann, R. E.; Burant, J. C.; Dapprich, S.; Millam, J. M.; Daniels, A. D.; Kudin, K. N.; Strain, M. C.; Farkas, O.; Tomasi, J.; Barone, V.; Cossi, M.; Cammi, R.; Mennucci, B.; Pomelli, C.; Adamo, C.; Clifford, S.; Ochterski, J.; Petersson, G. A.; Ayala, P. Y.; Cui, Q.; Morokuma, K.; Malick, D. K.; Rabuck, A. D.; Raghavachari, K.; Foresman, J. B.; Cioslowski, J.; Ortiz, J. V.; Stefanov, B. B.; Liu, G.; Liashenko, A.; Piskorz, P.; Komaromi, I.; Gomperts, R.; Martin, R. L.; Fox, D. J.; Keith, T.; Al-Laham, M. A.; Peng, C. Y.; Nanayakkara, A.; Gonzalez, C. Challacombe, M.; Gill, P. M. W.; Johnson, B.; Chen, W. Wong, M. W.; Andres, J. L.; Gonzales, C.; Head-Gordon, M.; Replogle, E. S.; Pople, J. A. *Gaussian 98*, Revision A.9; Gaussian, Inc.: Pittsburgh, PA, 1998.
(63) Becke, A. D. *J. Chem. Phys.* **1993**, *98*, 5648.
(64) Lee, C.; Yang, W.; Parr, R. G. *Phys. Rev. B* **1988**, *37*, 785.
(65) The Hay−Wadt valence basis sets and effective core potentials were obtained from the Extensible Computational Chemistry Environment Basis Set Database (available on the Internet at http://www.emsl.pnl.gov: 2080/forms/basisform.html), as developed and distributed by the Molecular Science Computing Facility, Environmental and Molecular Sciences Laboratory, which is part of the Pacific Northwest National Laborator, P.O. Box 999, Richland, WA 99352, and funded by the U.S. Department of Energy. For the original valence basis set and ECP reference, see: Hay, P. J.; Wadt, W. R. *J. Chem. Phys.* **1985**, *82*, 299.
(66) Glendening, E. D.; Feller, D.; Thompson, M. A. *J. Am. Chem. Soc.* **1994**, *116*, 10657.
(67) Walter, D.; Armentrout, P. B. *J. Am. Chem. Soc*. **1998**, *120*, 3176.
(68) Foresman, J. B.; Frisch, Æ. *Exploring Chemistry with Electronic Structure Methods*, 2nd ed.; Gaussian: Pittsburgh, PA, 1996.
(69) Boys, S. F.; Bernardi, R. *Mol. Phys.* **1979**, *19*, 553.
(70) Van Duijneveldt, F. B.; van Duijneveldt-van de Rijt, J. G. C. M.; van Lenthe, J. H. *Chem. Rev.* **1994**, *94*, 1873.
(71) Dzidic, I.; Kebarle, P. *J. Phys. Chem*. **1970**, *74*, 1466.
(72) Davidson, W. R.; Kebarle, P. *J. Am. Chem. Soc*. **1976**, *98*, 6125.
(73) Dalleska, N. F.; Tjelta, B. L.; Armentrout, P. B. *J. Phys. Chem*. **1994**, *98*, 4191.
(74) Feller, D.; Glendening, E. D.; Kendall, R. A.; Peterson, K. A. *J. Chem. Phys*. **1994**, *100*, 49881.
(75) See Walter, D.; Sievers, M. R.; Armentrout, P. B. *Int. J. Mass Spectrom. Ion Processes* **1998**, *175*, 93 for results of a $M^+(CO)_x$ + Ar (M = Li, Na, K) CID study in which the $M^+$−Ar thresholds were analyzed and found to be lower than the $M^+$−CO thresholds by the values of the $M^+$−Ar bond dissociation energies.
(76) Schultz, R. H.; Armentrout, P. B. *J. Phys. Chem.* **1993**, *97*, 596. Haynes, C. L.; Armentrout, P. B.; Perry, J. K.; Goddard, W. A., III. *J. Phys. Chem.* **1995**, *99*, 6340. Khan, F. A.; Steel, D. L.; Armentrout, P. B. *J. Phys. Chem.* **1995**, *99*, 7819. Meyer, F.; Chen, Y.-M.; Armentrout, P. B. *J. Am. Chem. Soc*. **1995**, *117*, 4071. Sievers, M.; Armentrout, P. B. *J. Phys. Chem.* **1995**, *99*, 8135. Goebel, S.; Haynes, C. L.; Khan, F. A.; Armentrout, P. B. *J. Am. Chem. Soc.* **1995**, *117*, 6994.
(77) More, M. B.; Glendening, E. D.; Ray, D.; Feller, D. Armentrout, P. B. *J. Phys. Chem.* **1996**, *100*, 1605.
(78) More, M. B.; Ray, D.; Armentrout, P. B. *J. Phys. Chem. A* **1997**, *101*, 1238.
(79) More, M. B.; Ray, D.; Armentrout, P. B. *J. Phys. Chem. A* **1997**, *101*, 4254.
(80) More, M. B.; Ray, D.; Armentrout, P. B. *J. Phys. Chem. A* **1997**, *101*, 7007.
(81) Lifshitz, C. *Adv. Mass Spectrom.* **1989**, *11*, 113.
(82) The metal−ring-centroid distance is defined as the distance from the metal atom to the central point within the aromatic ring that lies in the plane of the carbon atoms.
(83) Wilson, R. G.; Brewer, G. R. *Ion Beams: With Applications to Ion Implantation*; Wiley: New York, 1973; pp 118−124.
(84) See the Experimental Section in Rodgers.[36]
(85) Williams, J. H. *Acc. Chem. Res.* **1993**, *26*, 593.
(86) Armentrout, P. B. *Int. J. Mass Spectrom.* **2000**, *200*, 219.